A New PNS Code for Chemical Nonequilibrium Flows

D. K. Prabhu* and J. C. Tannehill†
Iowa State University, Ames, Iowa
and
J. G. Marvin‡
NASA Ames Research Center, Moffett Field, California

A new parabolized Navier-Stokes (PNS) code has been developed to compute the hypersonic laminar flow of a multicomponent, chemically reacting mixture of thermally perfect gases over two-dimensional and axisymmetric bodies. The new PNS code solves the gas dynamic and species conservation equations in a coupled manner using a noniterative, implicit, space-marching, finite-difference method. The conditions for well-posedness of the space-marching method have been derived from an eigenvalue analysis of the governing equations. The code has been used to compute the hypersonic laminar flow of chemically reacting air over wedges and cones. The results of these computations are in good agreement with the results of reacting boundary-layer calculations.

Introduction

THE recently proposed space transportation systems[1,2] have sparked a renewed interest in hypersonic aerothermodynamics. The high-temperature shock layers around these vehicles will have many complex relaxation phenomena, such as vibrational excitation, chemical reactions, and ionization, taking place within them. Furthermore, these relaxation process are likely to be far from equilibrium at the high operational altitudes of the vehicles. At present, simulation of such finite-rate processes in ground-based experimental facilities is difficult. Hence, numerical simulation is necessary to predict the aerothermodynamic environments around these vehicles. This is the focus of attention of several investigations today.

Several researchers[3-7] have used time-marching techniques to compute flowfields that are in thermochemical nonequilibrium. These methods require a substantial amount of computer time. Space-marching methods, on the other hand, require much less computer time and provide accurate solutions where applicable. In the past, inviscid chemical nonequilibrium flowfields around complex geometries such as the Space Shuttle Orbiter have been successfully analyzed[8-12] using space-marching methods. The success of Blottner[13,14] in computing viscous flows using boundary-layer methods has led to the development of a versatile boundary-layer code.[15] The seminal effort of Davis[16] has led to development and application[17-20] of the viscous shock-layer (VSL) equations. The VSL equations are uniformly valid in the shock layer and thus do not require specification of the flow conditions at the edge of the boundary layer. The equations, however, fail in the presence of crossflow separation because they are completely parabolic in both the streamwise and crossflow directions. This deficiency is overcome through the use of the parabolized Navier-Stokes (PNS) equations. The PNS equations are also uniformly valid in the shock layer but, unlike the VSL equations, do not fail in the presence of crossflow separation. Bhutta et al.[21] have recently used the PNS equations to compute chemical nonequilibrium flows around multiconic geometries.

The purpose of this paper is to describe the development of a new PNS code to compute nonequilibrium flowfields around two-dimensional and axisymmetric bodies. Only chemical nonequilibrium is considered, and thermal equilibrium is assumed. The coupled set of gas dynamic and species conservation equations is solved in a noniterative manner. This approach is different from that taken by Bhutta et al.,[21] who solved the gas dynamics and chemistry separately and used an iterative approach to couple the two. The present formulation also differs from previous viscous formulations in the form of the energy equation used. Since the gases that constitute the reacting mixture are thermally perfect, the energy equation is usually written in terms of the mixture temperature. While such a formulation leads to easier evaluation of thermodynamic and transport properties, it results in unwieldy source terms being added to the energy equation along with a loss of the conservation-law form. In the present formulation, the energy equation is written in terms of the total enthalpy of the mixture. Thus, the conservation-law form is retained. The mixture temperature is determined iteratively using the efficient Newton-Raphson method. This quadratically convergent method adds very little computing time.

The flow medium considered in the present computations is air consisting of five species. The code has been used to compute chemically reacting flowfields around wedges and cones. Results of the computations are compared with those of a reacting boundary-layer code.[15]

Governing Equations

PNS Equations

The equations governing the unsteady, laminar flow of a multicomponent gas in chemical and thermal nonequilibrium have been derived in great detail by Lee.[22] The two-dimensional/axisymmetric PNS equations are obtained from these equations by assuming that 1) the flow is steady, 2) there is only one temperature (thermal equilibrium), 3) there is no radiation or ionization, 4) the mass diffusion is binary and due to concentration gradients only, and 5) the viscous and diffusion effects in the streamwise direction are negligible. The resulting equations, which are expressed in (ξ,η) computational coordinates via the transformation $\xi = \xi(x,y)$, $\eta = \eta(x,y)$, can be written in nondimensional strong conservation-law form for an n-component system as

$$\boldsymbol{E}_\xi + \boldsymbol{F}_\eta + \boldsymbol{S}^i = \frac{1}{Re}(\boldsymbol{F}^v)_\eta + \frac{1}{Re}\boldsymbol{S}^v + \boldsymbol{S}^c \tag{1}$$

The $(n+3)$-component vector of conservation variables $\boldsymbol{Q}$ is

$$\boldsymbol{Q} = \{\rho,\rho u,\rho v,\rho H,\rho c_1,\rho c_2,\ldots,\rho c_{n-1}\}^T \tag{2}$$

Presented as Paper 87-0284 at the AIAA 25th Aerospace Sciences Meeting, Reno, NV, Jan. 12–15, 1987; received Jan. 12, 1987; revised July 29, 1987.

*Research Assistant, Department of Aerospace Engineering and Computational Fluid Dynamics Center. Currently with Eloret Institute, Sunnyvale, CA. Member AIAA.

†Manager, Computational Fluid Dynamics Center, and Professor, Department of Aerospace Engineering. Associate Fellow AIAA.

‡Chief, Experimental Fluid Dynamics Branch. Associate Fellow AIAA.

Note that the gas dynamic and chemistry variables are elements of the same vector.

For this choice of dependent variables, the $(n+3)$-component transformed inviscid flux vectors $\boldsymbol{E}$ and $\boldsymbol{F}$ are

$$\boldsymbol{E}=\frac{1}{J}\{\rho\hat{U},\rho u\hat{U}+p\xi_x,\rho v\hat{U}+p\xi_y,\rho H\hat{U},\rho c_1\hat{U},\ldots,\rho c_{n-1}\hat{U}\}^T$$

$$\boldsymbol{F}=\frac{1}{J}\{\rho\hat{V},\rho u\hat{V}+p\eta_x,\rho v\hat{V}+p\eta_y,\rho H\hat{V},\rho c_1\hat{V},\ldots,\rho c_{n-1}\hat{V}\}^T \quad (3)$$

where the contravariant velocity components are

$$\hat{U}=\xi_x u+\xi_y v$$
$$\hat{V}=\eta_x u+\eta_y v \quad (4)$$

The $(n+3)$-component transformed viscous flux vector $\boldsymbol{F}^v$ is

$$\boldsymbol{F}^v=\frac{1}{J}\begin{bmatrix}0\\ \ell_1 u_\eta+\ell_3 v_\eta\\ \ell_3 u_\eta+\ell_2 v_\eta\\ \frac{1}{2}(\ell_1-\ell_4)(u^2)_\eta+\frac{1}{2}(\ell_2-\ell_4)(v^2)_\eta+\ell_3(uv)_\eta+\\ \ell_4 H_\eta+(\ell_5-\ell_4)\sum_s h_s(c_s)_\eta\\ \ell_5(c_1)_\eta\\ \ell_5(c_2)_\eta\\ \vdots\\ \ell_5(c_{n-1})_\eta\end{bmatrix} \quad (5)$$

where the coefficients ℓ_1–ℓ_5 are

$$\ell_1=\mu\left(\frac{4}{3}\eta_x^2+\eta_y^2\right)\qquad \ell_4=\frac{\beta_2\kappa}{C_{pf}}(\eta_x^2+\eta_y^2)$$
$$\ell_2=\mu\left(\eta_x^2+\frac{4}{3}\eta_y^2\right)\qquad \ell_5=\beta_3\rho D(\eta_x^2+\eta_y^2) \quad (6)$$
$$\ell_3=\mu\left(\frac{1}{3}\eta_x\eta_y\right)$$

The inviscid source vector $\boldsymbol{S}^i$ for axisymmetric formulation is

$$\boldsymbol{S}^i=\frac{1}{yJ}\{\rho v,\rho uw,\rho v^2,\rho vH,\rho vc_1,\rho vc_2,\ldots,\rho vc_{n-1}\}^T \quad (7)$$

the viscous source vector $\boldsymbol{S}^v$ for the axisymmetric formulation is

$$\boldsymbol{S}^v=\frac{1}{yJ}\begin{bmatrix}0\\ -\frac{2}{3}y\eta_x(\mu v/y)_\eta+\mu(\eta_x v_\eta+\eta_y u_\eta)\\ -\frac{2}{3}y\eta_y(\mu v/y)_\eta+2\mu(\eta_y v_\eta-v/y)\\ -\frac{2}{3}y\eta_x(\mu uv/y)_\eta-\frac{2}{3}\eta_y(\mu v^2)_\eta+\\ \frac{1}{2}\left(\mu+\frac{\beta_2\kappa}{C_{pf}}\right)\eta_y(u^2+v^2)_\eta+\mu(u\eta_x v_\eta+v\eta_y u_\eta)-\\ \frac{2}{3}\mu v(\eta_x u_\eta+\eta_y v_\eta)_\eta-\frac{\beta_2\kappa}{C_{pf}}\eta_y H_\eta+\\ \left(\frac{\beta_2\kappa}{C_{pf}}-\beta_3\rho D\right)\eta_y\sum_s h_s(c_s)_\eta\\ \beta_3\rho D\eta_y(c_1)_\eta\\ \beta_3\rho D\eta_y(c_2)_\eta\\ \vdots\\ \beta_3\rho D\eta_y(c_{n-1})_\eta\end{bmatrix} \quad (8)$$

and the chemical source vector $\boldsymbol{S}^c$ is

$$\boldsymbol{S}^c=\frac{1}{J}\{0,0,0,0,\dot{w}_1,\ldots,\dot{w}_s,\ldots,\dot{w}_{n-1}\}^T \quad (9)$$

where $\dot{w}_s$ is the mass production rate of species s.

Only $(n-1)$ of the n species continuity equations are required because the sum of all the mass fractions is one. Therefore, the total number of conservation equations that need to be solved is $(n+3)$. The nth species continuity equation is replaced by the following algebraic equation:

$$c_n=1-\sum_{s=1}^{n-1}c_s \quad (10)$$

In addition to the preceding equations, the following equations are also used:

$$p=\frac{\beta_1\rho T}{M}=\beta_1\rho T\left(\sum_{s=1}^{n}\frac{c_s}{M_s}\right) \quad (11)$$

$$H=h+\frac{1}{2}(u^2+v^2) \quad (12)$$

Equation (11) is the equation of state for perfect gases, and Eq. (12) is the definition of the mixture total enthalpy.

In Eqs. (1–12), u, v, p, T, ρ, h, C_{pf}, M, μ, κ, and D represent the nondimensional velocity components in the x and y directions, pressure, temperature, density, enthalpy, frozen specific heat at constant pressure, molecular mass, viscosity, thermal conductivity, and binary diffusion coefficient, respectively. The following nondimensionalization has been employed in the present formulation (dimensional and freestream quantities are indicated by superscript * and subscript ∞, respectively):

$$x,y=\frac{x^*,y^*}{L^*}\qquad p=\frac{p^*}{p^*_\infty V^{*2}_\infty}\qquad \dot{w}_s=\frac{\dot{w}^*_s L^*}{\rho^*_\infty V^*_\infty}$$
$$u,v=\frac{u^*,v^*}{V^*_\infty}\qquad h=\frac{h^*}{V^{*2}_\infty}\qquad \mu=\frac{\mu^*}{\mu^*_\infty}$$
$$\rho=\frac{\rho^*}{\rho^*_\infty}\qquad M=\frac{M^*}{M^*_\infty}\qquad \kappa=\frac{\kappa^*}{\kappa^*_\infty} \quad (13)$$
$$T=\frac{T^*}{T^*_\infty}\qquad C_{pf}=\frac{C^*_{pf}T^*_\infty}{V^{*2}_\infty}\qquad D=\frac{D^*}{D^*_\infty}$$

and the other nondimensional quantities appearing in the equations are

$$Re=\frac{\rho^*_\infty V^*_\infty L^*}{\mu^*_\infty}\qquad \beta_2=\frac{\kappa^*_\infty T^*_\infty}{\mu^*_\infty V^{*2}_\infty}$$
$$\beta_1=\frac{R^*T^*_\infty}{M^*_\infty V^{*2}_\infty}\qquad \beta_3=\frac{\rho^*_\infty D^*_\infty}{\mu^*_\infty} \quad (14)$$

where Re is the Reynolds number based on the reference length L^* of unity and R^* is the universal gas constant (8314.34 J/kmol · K). The expressions for the Jacobian J and the metrics of the coordinate transformation ξ_x, ξ_y, η_x, and η_y are given in Ref. 23.

Gas Model, Thermodynamic, and Transport Properties

Gas Model

The chemical model used in the present calculations is air consisting of molecular oxygen (O_2), atomic oxygen (O), atomic nitrogen (N), nitric oxide (NO), and molecular nitrogen (N_2). These species are indexed $s=1$–5 in the order shown. The following reactions are considered between the constituent

species:

1) $O_2 + M_1 \rightleftharpoons 2O + M_1$
2) $N_2 + M_2 \rightleftharpoons 2N + M_2$
3) $N_2 + N \rightleftharpoons 2N + N$
4) $NO + M_3 \rightleftharpoons N + O + M_3$
5) $NO + O \rightleftharpoons O_2 + N$
6) $N_2 + O \rightleftharpoons NO + N$

where M_1, M_2, and M_3 are catalytic third bodies. The preceding model has five species ($n = 5$), six reactions, and eight reactants. The mass production rate of any species s of the gas model is calculated using expressions developed in Ref. 23, and all the necessary constants are obtained from Ref. 15.

Enthalpy and Specific Heat

The enthalpies and specific heats of the species are obtained from the following relations:

$$h_s^* = T^* \cdot C_{1,s}(T^*) + h_s^{0*}; \qquad \text{(J/kg)}$$

$$C_{p,s}^* = C_{2,s}(T^*); \qquad \text{(J/kg} \cdot \text{K)} \tag{15}$$

Tables of $C_{1,s}$ and $C_{2,s}$ as functions of T^* (K) are obtained from Ref. 15. Cubic spline interpolation is used in these tables. The enthalpy and frozen specific heat of the mixture are given by the following expressions:

$$h^* = \sum_{s=1}^{n} c_s h_s^*, \qquad C_{p_f}^* = \sum_{s=1}^{n} c_s C_{p,s}^* \tag{16}$$

Viscosity and Thermal Conductivity

The viscosity of species s is calculated from curve fits developed in Ref. 15. These curve fits are of the form

$$\mu_s^* = 0.1 \exp[(A_s \log_e T^* + B_s) \log_e T^* + C_s]; \qquad \text{(N} \cdot \text{s/m}^2\text{)} \tag{17}$$

where A_s, B_s, and C_s are constants. The thermal conductivity of species s is computed using Eucken's semiempirical formula

$$\kappa_s^* = \frac{\mu_s^* R^*}{M_s^*}\left(C_{p,s}^* \frac{M_s^*}{R^*} + \frac{5}{4}\right); \qquad \text{(W/m} \cdot \text{K)} \tag{18}$$

The viscosity and thermal conductivity of the mixture are calculated using Wilke's semiempirical mixing rule.[24]

Diffusion Coefficient

The binary Lewis numbers for all the species are assumed to be the same constant Le. The binary diffusion coefficient D^* is then computed from the definition

$$D^* = \frac{\kappa^* Le}{\rho^* C_{p_f}^*}; \qquad \text{(m}^2\text{/s)} \tag{19}$$

The dimensional thermodynamic and transport properties are nondimensionalized using Eq. (13) prior to their use in the code.

Streamwise Pressure Gradient

In their present form, the governing equations, Eq. (1), are hyperbolic-elliptic in the "streamwise" or marching direction ξ, and consequently the space-marching method of solution is ill-posed. An eigenvalue analysis (see Ref. 23 for details) of the governing equations shows that the single-sweep space-marching method of solution is well-posed if and only if 1) there is no axial flow separation in the domain of interest, 2) the local frozen Mach number is greater than unity in the inviscid part of the flowfield, and 3) only a fraction ω ($0 \le \omega \le 1$) of the streamwise pressure gradient is retained in the subsonic part of the flowfield. The magnitude of ω depends on the local frozen Mach number, and the final expression used is

$$\omega = \min\{1, \sigma M_f^{\xi 2}[1 + \chi(M_f^{\xi 2} - 1)]^{-1}\} \tag{20}$$

where σ ($0.8 \le \sigma \le 0.9$) is a factor of safety, M_f^{ξ} is the streamwise frozen Mach number, and $\chi = \beta_1 / MC_{p_f}$. Note that the entire streamwise pressure gradient term is retained if the streamwise frozen Mach number is greater than one.

The PNS equations after the introduction of ω can be written in compact form as

$$\boldsymbol{E}'_{\xi} + \boldsymbol{P}_{\xi} + \boldsymbol{F}_{\eta} + \boldsymbol{S}^i = \frac{1}{Re}(\boldsymbol{F}^v)_{\eta} + \frac{1}{Re}\boldsymbol{S}^v + \boldsymbol{S}^c \tag{21}$$

where

$$\boldsymbol{E}' = \frac{1}{J}\{\rho\hat{U}, \rho u\hat{U} + \omega p\xi_x, \rho v\hat{U} + \omega p\xi_y, \rho H\hat{U}, \rho c_1\hat{U}, \ldots, \rho c_{n-1}\hat{U}\}^T \tag{22}$$

$$\boldsymbol{P} = \frac{(1-\omega)p}{J}\{0, \xi_x, \xi_y, 0, 0, 0, \ldots, 0\}^T \tag{23}$$

The "elliptic" portion of the streamwise pressure gradient $\partial \boldsymbol{P}/\partial\xi$ is neglected within the subsonic portion of the boundary layer. As a result, the final set of equations becomes

$$\boldsymbol{E}'_{\xi} + \boldsymbol{F}_{\eta} + \boldsymbol{S}^i = \frac{1}{Re}(\boldsymbol{F}^v)_{\eta} + \frac{1}{Re}\boldsymbol{S}^v + \boldsymbol{S}^c \tag{24}$$

An implicit, noniterative, finite-difference scheme is used to solve the preceding system of equations.

Numerical Solution of PNS Equations

Finite-Difference Algorithm

The numerical algorithm used to solve the system of equations, Eq. (24), is an adaptation of the one developed by Tannehill et al.[26] The algorithm in delta-form is

$$\left\{A_{i,j} + \Delta\xi\frac{\partial}{\partial\eta}\left(B_{i,j} - \frac{1}{Re}M_{i,j}\right) - D_1\right\}\Delta_{i,j}\boldsymbol{Q} = -\Delta\xi\boldsymbol{E}'_{\xi}\Big|_{\boldsymbol{Q}} - \Delta\xi\frac{\partial}{\partial\eta}\left(\boldsymbol{F}_{i,j} - \frac{1}{Re}\boldsymbol{F}^v_{i,j}\right) - \Delta\xi\boldsymbol{S}^i_{i,j} + \frac{\Delta\xi}{Re}\boldsymbol{S}^v_{i,j} + \Delta\xi\boldsymbol{S}^c_{i,j} + D_2\boldsymbol{E}' \tag{25}$$

$$\boldsymbol{Q}_{i+1,j} = \boldsymbol{Q}_{i,j} + \Delta_{i,j}\boldsymbol{Q} \tag{26}$$

where

$$A = \left(\frac{\partial \boldsymbol{E}'}{\partial \boldsymbol{Q}}\right), \quad B = \left(\frac{\partial \boldsymbol{F}}{\partial \boldsymbol{Q}}\right), \quad M = \left(\frac{\partial \boldsymbol{F}^v}{\partial \boldsymbol{Q}}\right) \tag{27}$$

The subscript i refers to the station $\xi = i\Delta\xi$, and the subscript j refers to the point $\eta = (j-1)\Delta\eta$. The derivative $\partial/\partial\eta$ is replaced by the conventional three-point central-difference operator. The algorithm is first-order accurate in the ξ direction and second-order accurate in the η direction.

The Jacobian matrices A, B, and M are given in Ref. 23. In the linearization of the viscous flux, the transport properties are assumed to be locally constant. All the source terms have been lagged in the present formulation. The left-hand side of Eq. (25) corresponds to a block-tridiagonal system of equations. The blocks are square matrices of order ($n + 3$). For the five-species air model considered in the present calculations, the blocks are square matrices of order eight. The block-tridiagonal solver for the 8×8 blocks is developed along the same lines as the one by Steger[27] for 5×5 blocks. The second-order implicit and fourth-order explicit smoothing operators are D_1 and D_2, respectively. The forms of these operators can be found in Ref. 23.

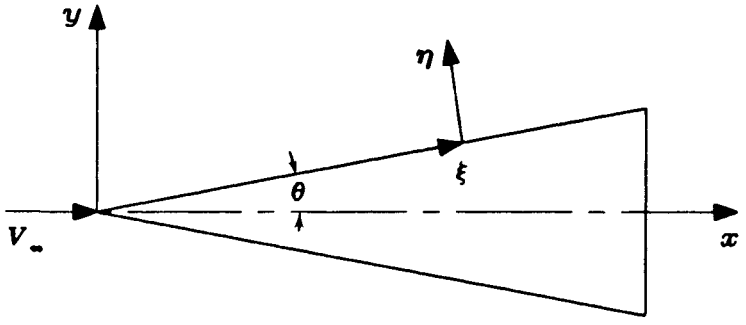

Fig. 1 Coordinate system.

Boundary Conditions

In the present work, the outer boundary is taken to be the freestream and the wall is taken to be the inner boundary. Any discontinuities in the flowfield are "captured" as a part of the solution.

The following nondimensional boundary conditions are imposed implicitly at the wall:

(1) $u = 0, \quad v = 0, \quad \partial p/\partial n = 0$

(2) $T = T_w$ (isothermal wall) or $\partial T/\partial n = 0$ (adiabatic wall)

(3) $c_s = c_{s\infty}$ (catalytic wall) or $\partial c_s/\partial n = 0$ (noncatalytic wall), $s = 1,2,...,n$

The nondimensional boundary conditions at the outer boundary are

(1) $u = 1, \quad v = 0$

(2) $T = 1, \quad \rho = 1, \quad c_s = c_{s\infty}, \quad s = 1,2,...,n$

Initial Conditions

The PNS equations require initial conditions in addition to the boundary conditions. The usual procedure is to use an initial data plane generated by a full Navier-Stokes code. For conical or pointed bodies, however, the present code generates it own starting solution. This starting solution is generated iteratively using a "stepback" procedure.[28] In this procedure, the viscous flow is assumed to be conical. Such an assumption is approximately valid for high Reynolds number flows over pointed bodies.[29] The flow variables are set to their freestream values, and the solution plane is marched from $\xi = \xi_0$ to $\xi = \xi_0 + \Delta\xi$ on a conical grid. The variables at the new station are scaled back to $\xi = \xi_0$. This procedure is continued until the L_2-norm of the change in variables is less than a preset tolerance.

Decoding

The primitive variables $\rho,u,v,H,c_1,...,c_{n-1}$ at station $i+1$ are easily obtained from the elements of $\boldsymbol{Q}_{i+1,j}$. The mass fraction of the nth species is computed using Eq. (10), and the static enthalpy of the mixture is computed using Eq. (12). For a given species distribution $c_1,c_2,...,c_n$ and mixture enthalpy h, the static temperature T^* is determined using the quadratically convergent Newton-Raphson (NR) method. The NR algorithm is

$$T^{*k+1} = T^{*k} - \frac{\sum_{s=1}^{n} c_s h_s^*(T^{*k}) - h^*}{\sum_{s=1}^{n} c_s C_{p,s}^*(T^{*k})} \tag{28}$$

where k is the index of iteration. The iterations are continued until the absolute value of the difference between two successive values of temperature is less than a given tolerance. Once the temperature is determined, the thermodynamic and transport properties are easily computed using the expressions given in the previous sections.

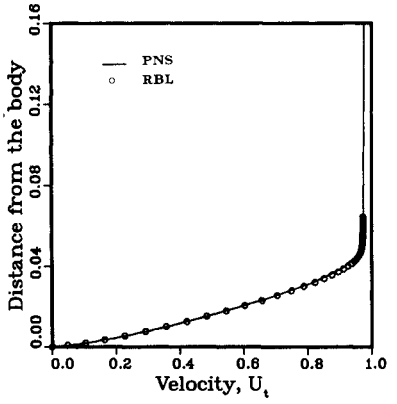

Fig. 2 Tangential velocity profiles at $x^*/L^* = 3.5$.

Grid Generation

An algebraic grid generation procedure is used in the present calculations. In this procedure, the point on the body surface and the point on the outer boundary are connected by a straight line, and the grid points are distributed on this line using a stretching function.[23] Grid stretching is necessary for good resolution of the subsonic viscous layer. The metrics are then computed using one-sided differences in the ξ direction and central differences in the η direction.

Numerical Results

In order to validate the present PNS code for chemical nonequilibrium flows, two test cases were computed. The coordinate system employed in the present calculations is shown in Fig. 1.

Test Case 1

The first test case computed was that of the hypersonic laminar flow of dissociating air over a 10-deg wedge. The altitude chosen was 60.96 km, where the ambient pressure and temperature are 20.35 N/m^2 and 252.6 K, respectively. The flow conditions were

$V_{2\infty}^* = 8100$ m/s

$T_w^* = 1200$ K and noncatalytic wall

$c_{1\infty} = 0.21$ and $c_{5\infty} = 0.79$

$Le = 1.4$

The computation was started at $x^*/L^* = 10^{-3}$ using initial conditions obtained from the "stepback" procedure. The solution was then marched to $x^*/L^* = 3.5$. The nondimensional marching step size was varied linearly from 5×10^{-4}–1.2×10^{-3}. The grid used in the calculations consisted of 67 points in the normal direction. The nondimensional distance of the first point away from the body surface was also varied linearly from 8×10^{-5}–3.5×10^{-4}, which determined the ap-

propriate value of the grid-stretching parameter. The grid lines were placed normal to the body, and the nondimensional height of the outer boundary was kept fixed at 0.75. The edge of the boundary layer was located approximately using total enthalpy as the criterion. The edge values of pressure, temperature, and velocity at the last station were then used as the uniform edge conditions for the reacting boundary-layer (RBL) code of Ref. 15.

Profiles of tangential velocity and temperature at $x^*/L^* = 3.5$ obtained from the two codes are compared in Figs. 2 and 3, respectively. The tangential velocity is defined as

$$U_t = u \cdot \cos\theta + v \cdot \sin\theta \tag{29}$$

The agreement between the two codes is very good, except over a small distance close to the boundary-layer edge. The O mass fraction and NO mass fraction at $x^*/L^* = 3.5$ obtained from the two codes are compared in Figs. 4 and 5, respectively. The PNS code predicts a greater amount of NO than the RBL code. It must be recalled here that the PNS equations contain a normal momentum equation. This permits interaction of the outer inviscid flow with the inner viscous region. At the altitude considered, this interaction is fairly strong because the Reynolds number is low. Consequently, the pressure is higher, which in turn implies a greater amount of dissociation.

The nondimensional pressure, skin-friction, and heat-transfer coefficients are defined as follows:

$$C_p = \frac{p_w^*}{\frac{1}{2}\rho_{ref}^* V_{ref}^{*2}}, \qquad C_f = \frac{\tau_w^*}{\frac{1}{2}\rho_{ref}^* V_{ref}^{*2}}, \qquad C_h = \frac{-q_w^*}{\frac{1}{2}\rho_{ref}^* V_{ref}^{*3}} \tag{30}$$

where the wall shear stress is computed from

$$\tau_w^* = -\mu_w^* \left.\frac{\partial V^*}{\partial n^*}\right|_w ; \quad (\mathrm{N/m^2}) \tag{31}$$

and the total heat transfer is computed from

$$q_w^* = -\kappa_w^* \left.\frac{\partial T^*}{\partial n^*}\right|_w - \rho_w^* D_w^* \sum_{s=1}^{n} h_s^* \left.\frac{\partial c_s}{\partial n^*}\right|_w ; \quad (\mathrm{W/m^2}) \tag{32}$$

The first term in Eq. (32) is the conductive heating rate, and the second term is the diffusive heating rate. The partial derivative $\partial/\partial n^*$ is taken in the direction normal to the body surface.

For this test case, the freestream conditions were chosen to be the reference conditions. In Fig. 6, the wall pressure coefficient is plotted against the axial distance. It is evident from the figure that the pressure predicted by the PNS code is higher than the edge pressure of the RBL code. It is also clearly seen that this pressure asymptotically reaches the edge pressure of the RBL code. The heat-transfer and skin-friction coefficients obtained from the two codes are plotted as functions of the distance along the code axis in Figs. 7 and 8, respectively.

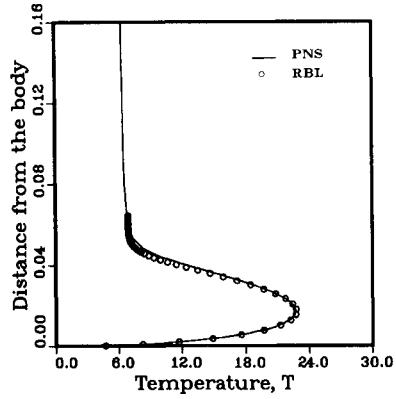

Fig. 3 Temperature profiles at $x^*/L^* = 3.5$.

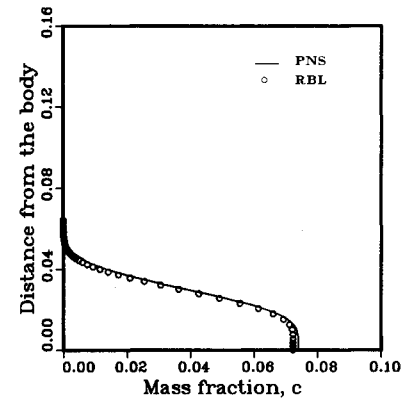

Fig. 4 O mass fraction profiles at $x^*/L^* = 3.5$.

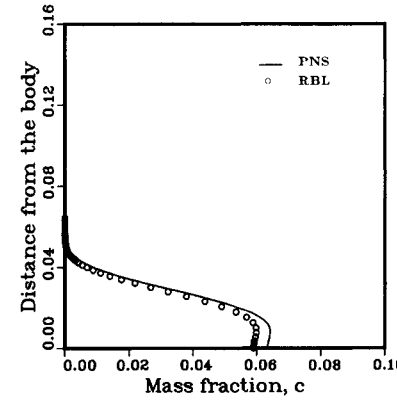

Fig. 5 NO mass fraction profiles at $x^*/L^* = 3.5$.

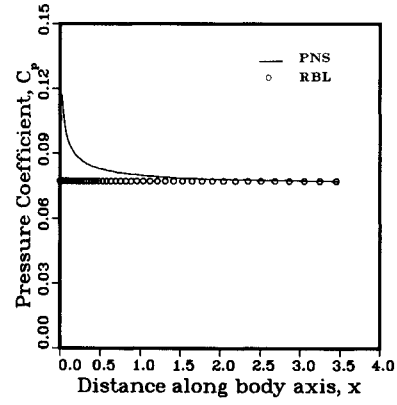

Fig. 6 Wall pressure coefficient comparison.

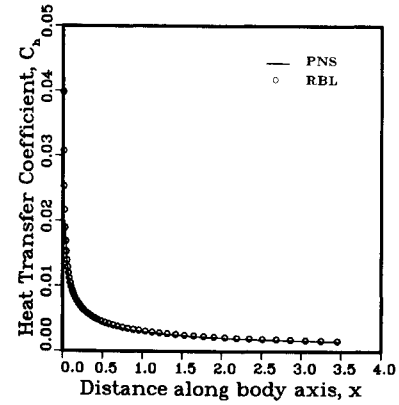

Fig. 7 Heat-transfer coefficient comparison.

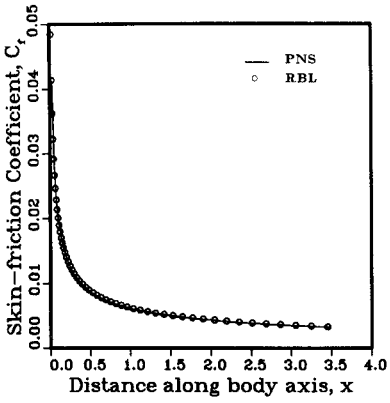

Fig. 8 Skin-friction coefficient comparison.

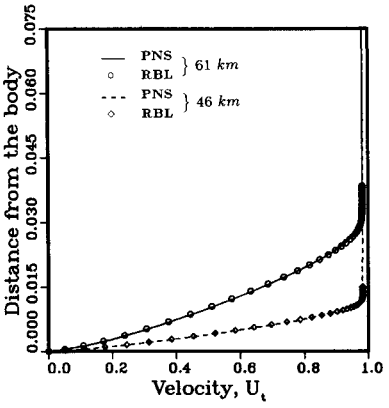

Fig. 9 Tangential velocity profiles at $x^*/L^* = 3.5$.

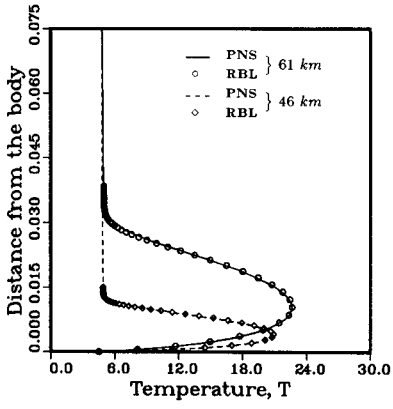

Fig. 10 Temperature profiles at $x^*/L^* = 3.5$.

The coefficients predicted by the two codes are in excellent agreement.

Test Case 2

The second test case computed was that of the hypersonic laminar flow of dissociating air over a 10-deg cone at two different altitudes. The first altitude chosen was 60.96 km, where the ambient pressure and temperature are 20.35 N/m^2 and 252.6 K, respectively, and the second altitude chosen was 45.72 km, where the ambient pressure and temperature are 136.7 N/m^2 and 266.2 K, respectively. The flow conditions were

$$V^*_\infty = 8100 \text{ m/s}$$

$$T^*_w = 1200 \text{ K and noncatalytic wall}$$

$$c_{1\infty} = 0.21 \quad \text{and} \quad c_{5\infty} = 0.79$$

$$Le = 1.4$$

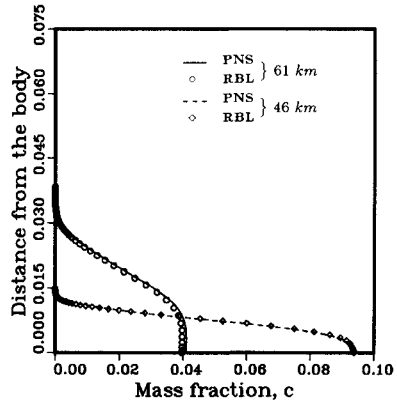

Fig. 11 O mass fraction profiles at $x^*/L^* = 3.5$.

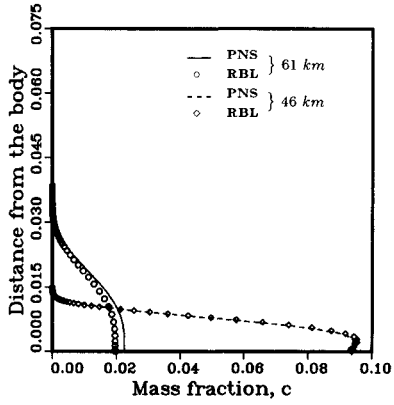

Fig. 12 NO mass fraction profiles at $x^*/L^* = 3.5$.

The computations for both the altitudes were started at $x^*/L^* = 10^{-3}$. The initial solutions were obtained using the "step-back" procedure. These initial solutions were marched to $x^*/L^* = 3.5$. The grids used in both calculations consisted of 67 points in the normal direction. For the higher altitude, the marching step size was varied linearly from 5×10^{-4}–1.2×10^{-3}, the distance of the first point away from the body surface was varied linearly from 8×10^{-5}–3.5×10^{-4}, the grid lines were placed normal to the body, and the height of the outer boundary was kept fixed at 0.5. For the lower altitude, the marching step size was varied linearly from 1×10^{-5}–1.2×10^{-3}, the distance of the first point away from the body surface was varied linearly from 5×10^{-6}–7×10^{-5}, the grid lines were placed normal to the body, and the height of the outer boundary was kept fixed at 0.35. As in the previous test case, the edge of the boundary layer was located approximately using total enthalpy as the criterion, and the edge values of pressure, temperature, and velocity at the last station were then used as the uniform edge conditions for the RBL code.[15]

The tangential velocity and temperature profiles at $x^*/L^* = 3.5$ are plotted in Figs. 9 and 10, respectively. The agreement between the two codes is excellent for both altitudes. The velocity and thermal boundary layers corresponding to the lower altitude are much thinner than those at the higher altitude. This is to be expected because the lower altitude corresponds to a higher Reynolds number. The O mass fraction and NO mass fraction profiles at $x^*/L^* = 3.5$ are displayed in Figs. 11 and 12, respectively. The amount of NO predicted by the PNS code is larger than the predicted by the boundary-layer code for the higher altitude. For the lower altitude, the amounts of NO predicted by the two codes are in good agreement. As mentioned earlier, the lower altitude corresponds to a higher Reynolds number, and consequently, the viscous boundary layer is quite thin. The interaction between the inviscid outer flow and the inner boundary layer is not as strong as that at the higher altitude.

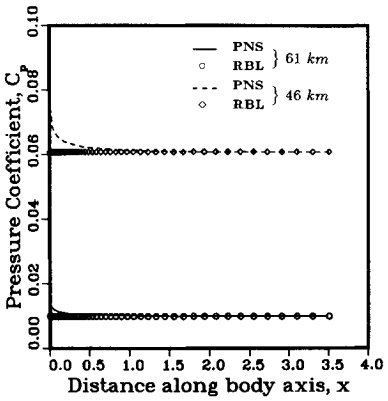

Fig. 13 Wall pressure coefficient comparison.

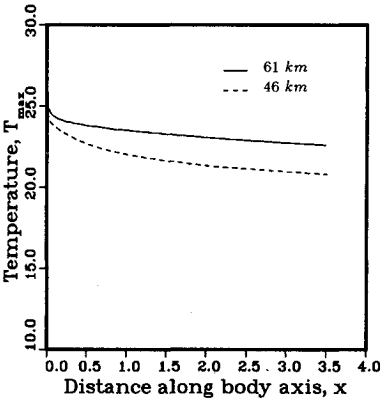

Fig. 16 Axial variation of peak temperature.

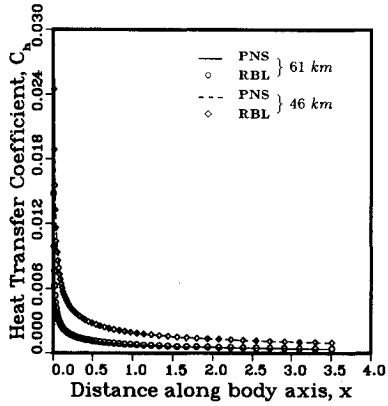

Fig. 14 Heat-transfer coefficient comparison.

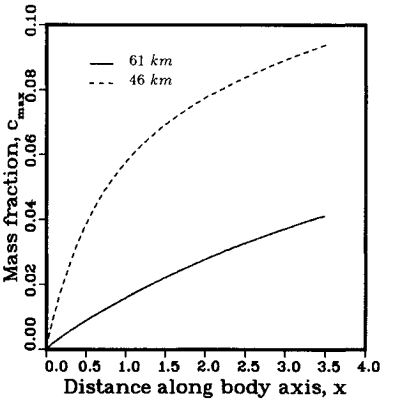

Fig. 17 Axial variation of peak O mass fraction.

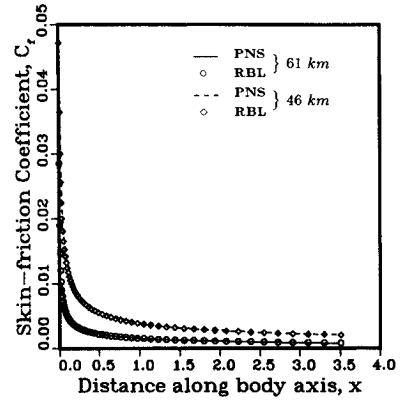

Fig. 15 Skin-friction coefficient comparison.

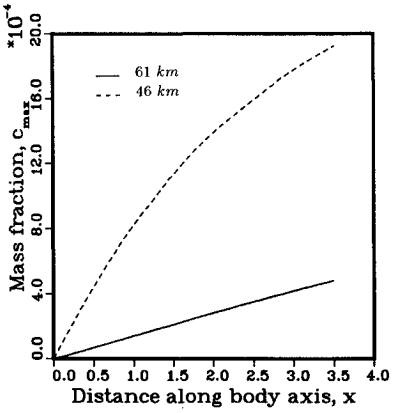

Fig. 18 Axial variation of peak N mass fraction.

The freestream conditions corresponding to the lower altitude were chosen as the reference conditions for the nondimensional coefficients. The computed surface pressure coefficients at the two altitudes are plotted as functions of the distance along the cone axis in Fig. 13. It is evident from the figure that the surface pressure asymptotically reaches a constant value. In Figs. 14 and 15, the computed heat-transfer and skin-friction coefficients, respectively, are displayed as functions of the axial distance. The agreement between the two codes is excellent at both altitudes. The figures show that the heat transfer and skin friction at the lower altitude are larger than those at the higher altitude.

In Fig. 16, the peak temperature in the viscous boundary layer is plotted as a function of the axial distance. The peak temperatures at the lower altitude are smaller than those at the higher altitude. This is to be expected since more dissociation takes place at the lower altitude. The peak O, N, and NO mass fractions in the flowfield are plotted against the axial distance in Figs. 17–19, respectively. As seen in these figures, significantly more dissociation takes place at the lower altitude than at the higher altitude.

The Damköhler number, which is the ratio of the fluid dynamic time scale to the chemical time scale, serves as a good measure of the "stiffness" of the chemically reacting system. For the altitudes considered in the present calculations, the Damköhler number is relatively small. This implies that the flow is closer to "frozen" flow since the chemical relaxation is very slow. Therefore, the step sizes chosen for the present cal-

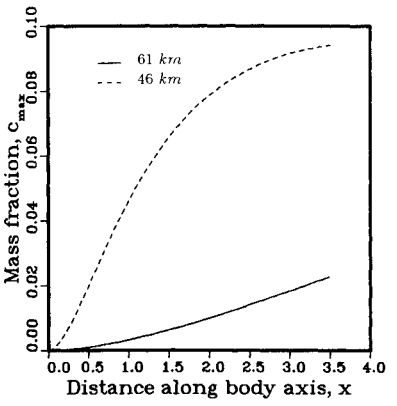

Fig. 19 Axial variation of peak NO mass fraction.

culations were adequate. A completely implicit treatment of the chemical source terms was found to have little or no effect on the results presented here.

All the computations were performed on the CRAY-XMP/48 computer at NASA Ames Research Center. Each test case involved 8×8 block matrices and required 2×10^{-4} s per grid point per step. The first test case required 4100 steps (55 s), and the second test case required 4100 (55 s) and 5800 (78 s) steps for the higher and lower altitudes, respectively.

Concluding Remarks

A new PNS code has been developed to compute the hypersonic laminar flow of chemically reacting air consisting of five species. Temperature variations of species, specific heats, and enthalpies were taken into account. A noniterative, implicit, space-marching, finite-difference method was used to solve the coupled set of gas dynamic and species conservation equations. The conditions for well-posedness of the space-marching method were derived from an eigenvalue analysis of the governing equations. In order to validate the code, two laminar test cases were computed, including hypersonic flow over a 10-deg wedge and hypersonic flow over a 10-deg cone at two different altitudes. The computed results were in very good agreement with those of reacting boundary-layer computations. The present work has been extended to compute three-dimensional flowfields around simple geometries, and the results are presented in Ref. 30.

Acknowledgments

This work was supported by NASA Ames Research Center under Grant NAG-2-245 and the Computational Fluid Dynamics Center, Iowa State University, Ames, Iowa. The authors wish to acknowledge Dr. F. G. Blottner of Sandia Laboratories, Albuquerque, New Mexico for providing the reacting boundary-layer code.

References

[1]Walberg, G. D., "A Survey of Aeroassisted Orbit Transfer," *Journal of Spacecraft and Rockets*, Vol. 22, Jan.–Feb. 1985, pp. 3–18.

[2]Howe, J. T., "Introductory Aerothermodynamics of Advanced Space Transportation Systems," *Journal of Spacecraft and Rockets*, Vol. 22, Jan.–Feb. 1985, pp. 104–111.

[3]Li, C. P., "Time-Dependent Solutions of Nonequilibrium Dissociating Gases Past a Blunt Body," *Journal of Spacecraft and Rockets*, Vol. 9, Aug. 1972, pp. 571–572.

[4]Park, C., "Problems of Rate Chemistry in the Flight Regimes of Aeroassisted Orbital Transfer Vehicles," *Progress in Aeronautics and Astronautics: Thermal Design of Aeroassisted Orbit Transfer Vehicles*, Vol. 96, edited by H. F. Nelson, AIAA, New York, 1985, pp. 511–537.

[5]Park, C., "Convergence of Computation of Chemically Reacting Flows," *Progress in Aeronautics and Astronautics: Thermophysical Aspects of Re-entry Flows*, Vol. 103, edited by J. N. Moss and C. D. Scott, AIAA, New York, 1986, pp. 478–513.

[6]Gnoffo, P. A. and McCandless, R. S., "Three-Dimensional AOTV Flowfields in Chemical Nonequilibrium," AIAA Paper 86-0230, Jan. 1986.

[7]Li, C. P., "Implicit Methods for Computing Chemically Reacting Flow," NASA TM-58274, Sept. 1986.

[8]Marrone, P. V. and Garr, L. J., "Invisicid, Nonequilibrium Flow Behind Bow and Normal Shock Waves," Vols. 1 and 2, Cornell Aeronautics Laboratory, Repts. QM-1616-A-12(I) and (II), May 1963.

[9]Kliegel, J. R., Peters, R. L., and Lee, J. T., "Characteristics Solution for Nonequilibrium Flow Fields About Axisymmetric Bodies," Vols. 1 and 2, TRW Space Technology Laboratories, Inc., Repts. 6453-6001-KU-000 and 6453-6002-KU-000, July 1964.

[10]Davy, W. C. and Reinhardt, W. A., "Computation of Shuttle Nonequilibrium Flow Fields on a Parallel Processor," *Aerodynamic Analyses Requiring Advanced Computers, Part II*, NASA SP-347, 1975, pp. 1351–1376.

[11]Rizzi, A. W. and Bailey, H. E., "A Generalized Hyperbolic Marching Method for Chemically Reacting 3-D Supersonic Flow using a Splitting Technique," *Proceedings of AIAA 2nd Computational Fluid Dynamics Conference*, June 1975.

[12]Rakich, J. V., Bailey, H. E., and Park, C., "Computation of Nonequilibrium Supersonic Three-Dimensional Inviscid Flow over Blunt-Nosed Bodies," *AIAA Journal*, Vol. 21, June 1983, pp. 834–841.

[13]Blottner, F. G., "Chemical Nonequilibrium Boundary Layer," *AIAA Journal*, Vol. 2, Feb. 1964, pp. 232–240.

[14]Blottner, F. G., "Nonequilibrium Laminar Boundary Layer of Ionized Air," *AIAA Journal*, Vol. 2, Nov. 1964, pp. 1921–1927.

[15]Blottner, F. G., Johnson, M., and Ellis, M., "Chemically Reacting Viscous Flow Program for Multi-Component Gas Mixtures," Sandia Laboratories, Albuquerque, NM, Rept. SC-RR-70-754, Dec. 1971.

[16]Davis, R. T., "Chemically Reacting Flow of a Binary Mixture Past a Blunt Body," AIAA Paper 70-805, July 1970.

[17]Moss, J. N., "Reacting Viscous Shock-Layer Solutions with Multicomponent Diffusion and Mass Injection," NASA TR R-411, June 1974.

[18]Miner, E. W. and Lewis, C. H., "Hypersonic Ionizing Air Viscous Shock-Layer Flows over Nonanalytic Blunt Bodies," NASA CR-2550, May 1975.

[19]Shinn, J. L., Moss, J. N., and Simmonds, A. L., "Vicous-Shock-Layer Heating Analysis for the Shuttle Windward Plane with Surface Finite Catalytic Recombination Rate," AIAA Paper 84-0842, June 1982.

[20]Swaminathan, S., Kim, M. D., and Lewis, C. H., "Nonequilibrium Viscous Shock-Layer Flows over Blunt Sphere-Cones at Angles-of-Attack," AIAA Paper 82-0825, June 1982.

[21]Bhutta, B. A., Lewis, C. H., and Kautz, F. A. II, "A Fast Fully-Iterative Parabolized Navier-Stokes Scheme for Chemically-Reacting Reentry Flows," AIAA Paper 85-0926, June 1985.

[22]Lee, J. H., "Basic Governing Equations for the Flight Regimes of Aeroassisted Orbital Transfer Vehicles," *Progress in Aeronautics and Astronautics: Thermal Design of Aeroassisted Orbit Transfer Vehicles*, Vol. 96, edited by H. F. Nelson, AIAA, New York, 1985, pp. 3–53.

[23]Prabhu, D. K., Tannehill, J. C., and Marvin, J. G., "A New PNS Code for Chemical Nonequilibrium Flows," AIAA Paper 87-0284, Jan. 1987.

[24]Wilke, C. R., "A Viscosity Equation for Gas Mixtures," *Journal of Chemical Physics*, Vol. 18, April 1950, p. 517.

[25]Vigneron, Y. C., Rakich, J. V., and Tannehill, J. C., "Calculation of Supersonic Flow over Delta Wings with Sharp Subsonic Leading Edges," AIAA Paper 78-1137, July 1978.

[26]Tannehill, J. C., Venkatapathy, E., and Rakich, J. V., "Numerical Solution of Supersonic Viscous Flow over Blunt Delta Wings," *AIAA Journal*, Vol. 20, Feb. 1982, pp. 203–210.

[27]Steger, J. L., "Implicit Finite-Difference Simulation of Flow About Arbitrary Geometries with Applications to Airfoils," AIAA Paper 77-665, June 1977.

[28]Schiff, L. B. and Steger, J. L., "Numerical Simulations of Steady Supersonic Viscous Flow," AIAA Paper 79-0130, Jan. 1979.

[29]Anderson, D. A., Tannehill, J. C., and Pletcher, R. H., "*Computational Fluid Mechanics and Heat Transfer*," Hemisphere Publishing Corp, New York, 1984.

[30]Prabhu, D. K., Tannehill, J. C., and Marvin, J. G., "A New PNS Code for Three-Dimensional Chemically Reacting Flows," AIAA Paper 87-1472, June 1987.